3D aeroacoustic simulations of a flow-excited Helmholtz resonator

Péter Rucz[1]

[1] *Budapest University of Technology and Economics, Budapest, Hungary, Email: rucz@hit.bme.hu*

Introduction

The flow-excited Helmholtz resonator is a classical example of acoustical resonance induced by fluid flow. When the frequency of the hydrodynamic instabilities of the shear layer formed at the orifice of the cavity is close to the natural resonance frequency of the resonator, high amplitude pressure oscillations occur, and a strong acoustical feedback on the shear layer is observed. Similar phenomena of sound production are also responsible for the noise amplification in ventilation ducts with side branches and the sound generation of air reed wind instruments, for example.

This paper presents three-dimensional aeroacoustic simulations of a Helmholtz resonator excited by grazing flow in different configurations. First, the oscillations of the shear layer are analyzed without acoustical feedback using incompressible simulations. Then, the acoustical impulse response of the resonator is evaluated in the absence of the flow excitation. Finally, flow induced acoustical resonance is examined at different flow speeds by means of compressible large eddy simulations. All cases are implemented using the OpenFOAM software package. The results of numerical simulations are compared with previous 2D models and experimental as well as computational data published earlier by other authors. The examinations presented in this paper continue those discussed in [1].

Physical model

The left hand side of Figure 1 sketches the configuration of a Helmholtz resonator excited by grazing flow. The flow coming from the left reaches the orifice of the resonator where a shear layer develops. Even without the acoustical feedback of the resonator, the layer exhibits hydrodynamic self-oscillations whose frequencies depend on the length of the orifice L, the freestream flow velocity U, and the profile of the boundary layer at the leading edge of the orifice. The oscillating shear layer also provides hydrodynamic forcing on the acoustical resonator. Finally, the pressure response of the resonator exerts force on the shear layer in the cross-stream direction. Hence, a hydrodynamic–acoustic feedback loop is formed by which the system is capable of producing self-sustained oscillations.

The lumped element model of the resonator is depicted in the right hand side of Figure 1. The damped mass–spring oscillator is characterized by the stiffness K of the air volume enclosed in the cavity, the resistance R representing the radiation and wall losses, and the mass of air M oscillating in the neck having an effective length l_e that also includes the correction effect of the radiation

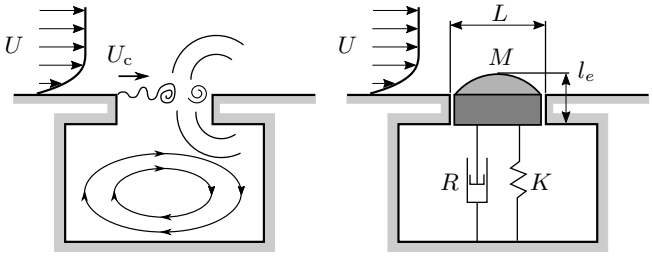

Figure 1: Sketch of the flow configuration (left) and the lumped element acoustical model (right).

impedance. Following [2], the transfer function H of the resonator is written in the frequency domain as

$$H(f) = \frac{p_{\mathrm{res}}}{p_{\mathrm{exc}}} = \frac{K}{-4\pi^2 f^2 M + \mathrm{j}2\pi f R + K}, \qquad (1)$$

with p_{exc} denoting the excitation pressure and p_{res} standing for the pressure inside the resonator. The resonance frequency and the quality factor of the resonator are expressed from the lumped parameters as $f_{\mathrm{hr}} = \sqrt{K/M}/2\pi$ and $Q = 2\pi f_{\mathrm{hr}} M/R$. In terms of non-dimensional frequencies $f^* = f/f_{\mathrm{hr}}$ the transfer function (1) reads as

$$H(f^*) = \frac{1}{-f^{*2} + \mathrm{j}f^*/Q + 1}. \qquad (2)$$

In the sequel, the above quantities are estimated from impulse response simulations, while the transfer function is exploited for the prediction of resonance frequencies.

Simulation arrangement

The examined geometry is depicted in Figure 2. The configuration consists of a rectangular wind channel and a box-shaped resonator that is attached to the bottom of the channel. The two parts are connected by a square orifice that functions as the neck of the resonator. The same configuration were used in the measurements of Ma *et al.* [2], the discrete vortex model (DVM) of Dai *et al.* [3], and the 3D LES study by Ghanadi *et al.* [4]. The only difference in the geometry in these works is the edge of the resonator: in the measurements a sharp edge with 30° was set, in the DVM the thickness of the plate is neglected, and in the 3D simulations blunt 90° edges were modeled. Here, the latter variant is examined.

A structured mesh of the model shown in Figure 2 is created. As a spatially constant inlet velocity is applied, an additional length of 1.5 m is added to the inlet side of the channel to have a developed boundary layer profile at the leading edge of the orifice. The minimum edge sizes, used at the edges of the orifice, are $\Delta x = 0.6\,\mathrm{mm}$, $\Delta y = 0.4\,\mathrm{mm}$ and $\Delta z = 0.8\,\mathrm{mm}$, while the maximum

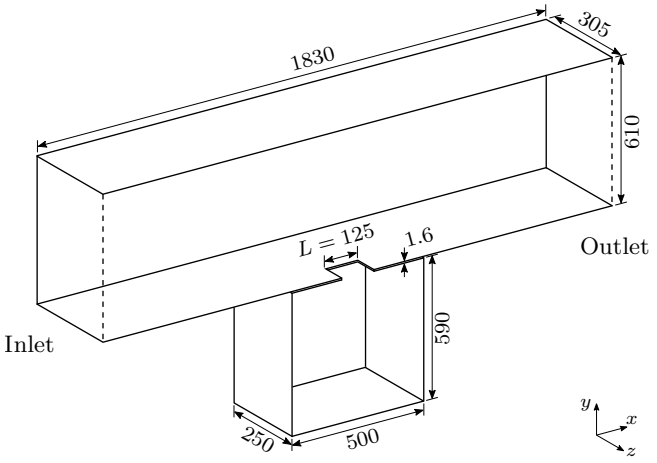

Figure 2: Geometry of the simulated Helmholtz resonator and wind channel. All sizes are given in mm units.

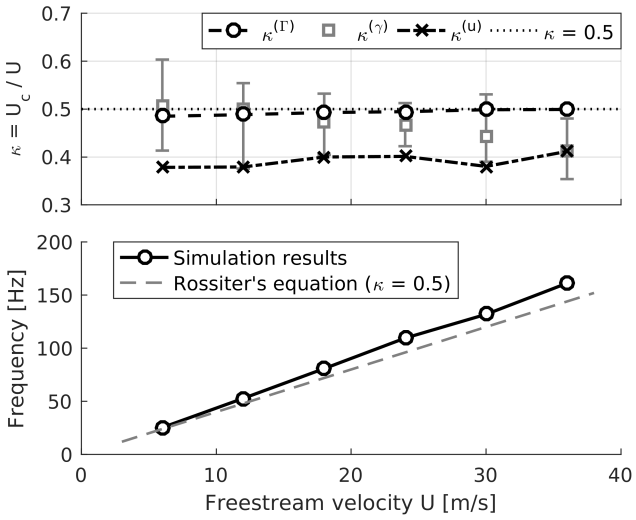

Figure 3: Comparison of the convection velocities κ (top) and the shear layer oscillation frequencies (bottom).

edge length is 20 mm along all axes. The edge size of two adjacent elements differ up to a maximum of 7.5%. The final mesh had ≈ 2.4 M elements.

At the inlet a time varying velocity is set, that smoothly increases from zero to the final freestream velocity U in 0.25 s using a raised cosine function. The top and side walls of the wind channel are assumed to be frictionless and a slip boundary condition is used there, while at other walls no-slip is prescribed. A symmetry plane boundary condition is applied at the $z = 0$ plane. Turbulence not resolved by the mesh is modeled using the wall adaptive large eddy simulation method (WALE) [5] both in incompressible and compressible cases. Postprocessing is facilitated by using several pressure probes inside the resonator and the channel and a number of velocity probes across the orifice. All simulations were carried out using `OpenFOAM-plus` [6].

Shear layer oscillations

Oscillations of the shear layer are examined first without acoustical feedback using incompressible CFD. The frequency f of the oscillations is evaluated from the velocity probe data and compared to Rossiter's relation:

$$\frac{f_n L}{U} = \frac{n-\alpha}{\mathrm{Ma} + 1/\kappa} \quad \rightarrow \quad f_1 \approx \frac{U}{L}\kappa. \tag{3}$$

Here n refers to the nth hydrodynamic mode, Ma stands for the Mach number, $\kappa = U_\mathrm{c}/U$ is the nondimensional convection speed of perturbations, and the phase delay of the feedback is taken as $\alpha = 0$. In the incompressible case the linear relation on the right side of (3) is retained.

Different approaches exist for estimating κ. A simple method used in [1] is to average the streamwise velocity u_x across the orifice for a whole time period T:

$$\kappa^{(u)} = \frac{1}{ULT}\int_0^T \int_0^L u_x(x,t)\,\mathrm{d}x\,\mathrm{d}t. \tag{4}$$

Two alternative methods are also proposed in [2]. First, the convection speed of vorticity as a whole can be evaluated using the vorticity ω_z as

$$\kappa^{(\Gamma)} = \frac{1}{UT}\int_0^T \frac{\int u_x(x,y,t)\omega_z(x,y,t)\,\mathrm{d}S}{\int \omega_z(x,y,t)\,\mathrm{d}S}\,\mathrm{d}t, \tag{5}$$

where S is the surface of an analysis window of size $L \times 0.75L$ centered at the orifice. The circulation $\Gamma(t)$ appears in the denominator. Finally, a third approach is to evaluate the circulation density γ in the analysis window as

$$\gamma(x,t) = \int \omega_z(x,y,t)\,\mathrm{d}y, \tag{6}$$

and then derive $\kappa^{(\gamma)}$ from phase averaged values of γ.

The top diagram of Figure 3 shows different approximations of κ evaluated from the CFD results at various flow speeds. As observed, the three methods lead to different results. $\kappa^{(u)} \approx 0.4$ is found with small deviations, while $\kappa^{(\Gamma)} \approx 0.5$ at all flow speeds. It was difficult to evaluate $\kappa^{(\gamma)}$ from the CFD results and while the mean values are between $0.4 \leq \kappa^{(\gamma)} \leq 0.5$, the uncertainty is large, which is attributed to the strictly limited number of phase averages in the exported CFD data.

The bottom plot of Figure 3 displays the oscillation frequencies resulting from the LES compared to those obtained from (3). In the incompressible simulations always the first mode was observed. The linear trend predicted by (3) is well captured by the simulations, however, the CFD gives slightly higher frequencies, especially at higher velocities, with the deviations ranging from 5% to 11%.

The acoustical response of the resonator

To examine the acoustical properties of the resonator, its impulse response was determined. In this case the bottom resonator wall became the inlet of the system, while the two ends of the simulated channel both became outlets, where wave transmissive boundary conditions are

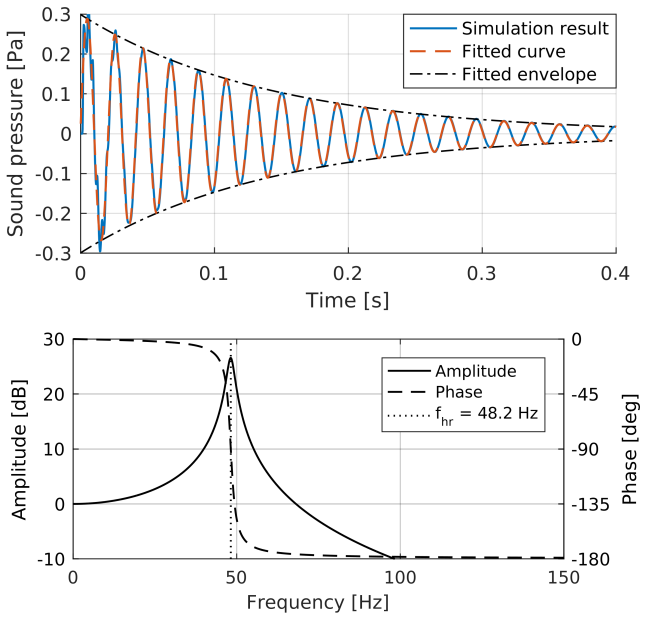

Figure 4: Top: Simulated impulse response of the resonator. Bottom: Bode plot of the transfer function H calculated from the fitted parameters.

Method	f_{hr} [Hz]	Q
Measurement [2]	46	11
3D Helmholtz FEM	55	33
2D Navier – Stokes [1]	55	12
3D Navier – Stokes	48	21

Table 1: Acoustical properties of the Helmholtz resonator estimated by different methods

applied. At the inlet a plenum pressure boundary condition was prescribed which creates a zero-dimensional model of an enclosed volume of gas upstream of the inlet [6]. The response of the resonator is recorded by a pressure probe located at the middle of the orifice.

Figure 4 shows the simulated impulse response of the resonator. After some irregularities in the first few periods, a smooth, exponentially decaying sinous response is attained. The resonance frequency f_{hr} and the quality factor Q are estimated by curve fitting. The resulting transfer function H is plotted in the bottom diagram of Figure 4. For the sake of comparison, Table 1 shows the properties of the resonator estimated using different methods. As seen, the resonance frequency predicted by the present 3D Navier – Stokes model matches quite well with the measurements, while the simulated quality factor is greater than the measured one. Apparently, frequency domain simulation using standard Helmholtz FEM gives a higher resonance frequency and Q-factor.

Flow-excited resonance

Following [2] the phase lock condition for self-sustained resonance can be written as

$$\frac{2\pi f_{\mathrm{p}}^*}{U_{\mathrm{c}}^*} - \angle H(f_{\mathrm{p}}^*) - \frac{\pi}{2} = 2n\pi \qquad n = 1, 2, \ldots \qquad (7)$$

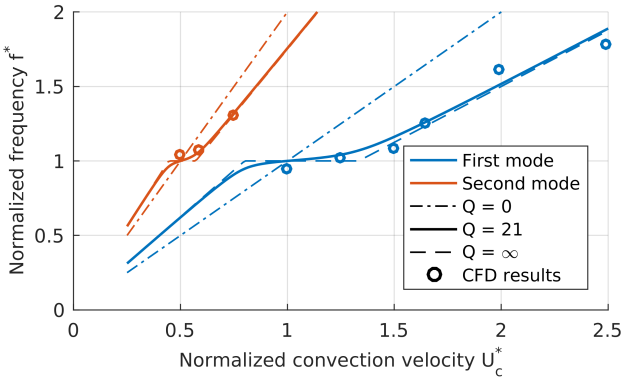

Figure 5: Estimated frequencies of flow excited resonance compared with simulation results

with f_{p}^* denoting the predicted resonance frequency normalized by f_{hr} and $U_{\mathrm{c}}^* = U_{\mathrm{c}}/(f_{\mathrm{hr}}L)$. The first term on the left hand side represents the phase delay of the perturbation propagation in the shear layer, while the second term is the delay of the acoustical feedback from the resonator pressure p_{res} on the excitation pressure p_{exc}. The shift of $\pi/2$ converts velocity into displacement. In the steady state, the total phase delay on the left hand side adds up to n complete cycles when the nth hydrodynamic mode is excited.

Equation (7) can be solved graphically in order to attain the predicted resonace frequency f_{p}^* at a given convection velocity U_{c}^*. Figure 5 displays the predicted resonance frequencies compared to those obtained from the LES. The solid lines show the expected frequencies with $Q = 21$ that resulted from the impulse response simulations. As seen, around $U_{\mathrm{c}}^* = 1$ and $U_{\mathrm{c}}^* = 0.5$ phase locking occurs and flat plateaus are observed in the expected frequency. The theoretical limiting cases of $Q = 0$ and $Q \to \infty$ are also displayed.

For the evaluation of the CFD results the convection velocity U_{c} was evaluated based on (5). The frequencies extracted from the simulation results are in good agreement with the expectations. In accordance with [2, 4] at lower flow speeds ($6\,\mathrm{m/s} \leq U \leq 9\,\mathrm{m/s}$) both modes are observed in the simulations, but the frequency locking occurs at the second mode.

Figure 6 shows the pressure spectra at the bottom of the resonator at three characteristic flow speeds. The nondimensional velocities are defined as $U^* = U/(f_{\mathrm{hr}}L)$. The simulation results are evaluated in short time windows and hence the spectral resolution is lower compared to the measured spectra. A good agreement of measured and simulated spectra is found in all three cases.

At $U^* = 1.2$ the excitation of both the first (at $f^* \approx 0.5$) and second (at $f^* \approx 1.0$) hydrodynamic modes is visible. The amplitude of both modes matches the measurement quite well. In the simulation, the third peak at $f^* \approx 1.6$ is stronger than that in the measurement by about 20 dB, however, this peak is already more than 20 dB lower than the strongest peak of the second mode.

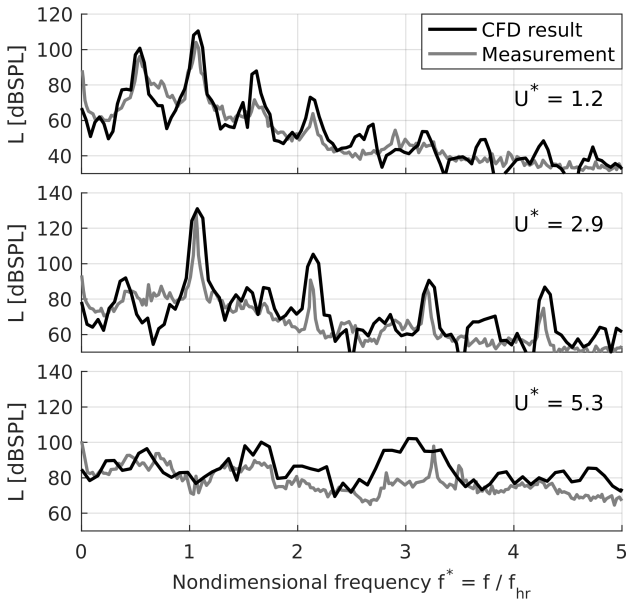

Figure 6: Pressure spectra at the bottom of the resonator at different flow speeds. Comparison of LES results to measurements of Ma *et al* [2].

With increasing the freestream velocity, the first hydrodynamic mode becomes dominant, as observed at $U^* = 2.9$. The frequency and the amplitude of the first mode agrees very well with the measured values. In this case the first few harmonics are also clearly visible in the spectrum. The amplitude of the second harmonic is about 15 dB higher in the simulation.

Further increasing the freestream velocity, strong flow-induced resonance is no longer observed. As seen, the spectra at $U^* = 5.3$ do not have tonal peaks, broadband noise is visible instead. The measured and simulated noise baselines are in good agreement, with the highest deviations observed around $f^* \approx 3$.

Conclusions

Three-dimensional LES of a Helmholtz resonator excited by grazing flow was discussed in the paper. The approach pursued in the paper enables examining the shear layer oscillations, the impulse response of the resonator, and flow-excited resonance independent of each other, but using the same simulation framework. CFD simulation results were compared to theoretical analysis and measurements reported in [2] with discussing the observed tendencies. The simulations reproduce the observations of the measurements quite well.

It is worth discussing some of the similarities and differences to the previous 2D study [1]. By choosing the 2D model, the choices available for turbulence modeling are limited: in the 2D study k-ω SST URANS simulations were used, while in the 3D case a more sophisticated LES is utilized. As far as the acoustical properties of the resonator are concerned, the radiation characteristics cannot be reproduced properly by the 2D model, and as it was shown, the Helmholtz resonance frequency is much closer to the measured value in the 3D simulation. At higher flow speeds, a significant recirculation of the flow was observed inside the resonator in case of the 2D model. Finally, in the 2D arrangement, an acoustical damping layer had to be attached at the top wall of the channel to prevent the channel section from the inlet to the orifice from functioning as an efficient $\lambda/4$ resonator and corrupting the resonance frequency of the system. The latter two phenomena were not observed in case of 3D simulations. This is explained by the fact that the 2D setup cannot capture that the depth of the orifice is only a fraction of that of the resonator or the channel. Therefore, the flow cannot expand along the z axis, leading to strong recirculation. At the same time, as the "depth" of the orifice is same as that of the channel in the 2D model, the acoustical excitation of the channel at the orifice is much more efficient and resonance is more likely to occur inside the channel. In summary, it can be said that the observed dissimilarities are in accordance with the a priori expectations.

Acknowledgments

The author gratefully acknowledges the support of the Bolyai János research grant provided by the Hungarian Academy of Sciences.

Supported by the ÚNKP–19-4 New National Excellence Program of the Ministry for Innovation and Technology.

References

[1] P. Rucz. Aeroacoustic simulation of a flow-excited Helmholtz resonator using OpenFOAM. In S. Spors and F.-H. Wurm, editors, *DAGA2019 45. Deutsche Jahrestagung für Akustik*, pages 1426–1429, Rostock, Germany, 2019. Deutsche Gesellschaft für Akustik e.V. (DEGA).

[2] R. Ma, P. E. Slaboch, and S. C. Morris. Fluid mechanics of the flow-excited Helmholtz resonator. *Journal of Fluid Mechanics*, 623:1–26, 2009.

[3] X. Dai, X. Jing, and X. Sun. Flow-exciated acoustic resonance of a Helmholtz resonator: Discrete vortex model compared to experiments. *Physics of Fluids*, 27:057102–1–24, 2015.

[4] F. Ghanadi, M. Arjomandi, B. Cazzolato, and A. Zander. Understanding of the flow behaviour on a Helmholtz resonator excited by grazing flow. *International Journal of Computational Fluid Dynamics*, 28(5):1–13, 2014.

[5] F. Nicoud and F. Ducros. Subgrid-scale stress modelling based on the square of the velocity gradient tensor. *Flow Turbulence Combust*, 62:183–200, 1999.

[6] OpenCFD release OpenFOAM v1912. `https://www.openfoam.com/releases/openfoam-v1912/` Last visited: March 30, 2020.